# Influence of longitudinal structural connectivity on seismic performance of three-hinged precast arch culverts

AUTHOR(S):

Miyazaki, Yuusuke; Sawamura, Yasuo; Kishida, Kiyoshi; Kimura, Makoto

HOSTED BY
ELSEVIER
Available online at www.sciencedirect.com
ScienceDirect
Soils and Foundations 61 (2021) 1681–1698
SOILS AND FOUNDATIONS
www.elsevier.com/locate/sandf

Technical Paper

# Influence of longitudinal structural connectivity on seismic performance of three-hinged precast arch culverts

Yuusuke Miyazaki [a,*], Yasuo Sawamura [a], Kiyoshi Kishida [a], Makoto Kimura [b]

[a] *Department of Urban Management, Kyoto University, C Cluster, Kyoto daigaku-katsura Nishikyo-ku, Kyoto 615-8540, Japan*
[b] *Department of Civil and Earth Resources Engineering, Kyoto University, C Cluster, Kyoto daigaku-katsura Nishikyo-ku, Kyoto 615-8540, Japan*

Received 16 June 2021; received in revised form 23 September 2021; accepted 6 October 2021
Available online 16 November 2021

**Abstract**

The hinge type of precast concrete arch culvert was introduced to Japan from France in the 1990s in consideration of the saving of labor, shortening of the construction period, and high quality control of the concrete members. However, due to the 2011 off the Pacific Coast of Tohoku Earthquake (March 11, 2011), the three-hinged precast arch culverts that had been constructed in Japan at the beginning of the period when precast arch culverts were firstly introduced, suffered damage, which spoiled their serviceability. According to the extent of the damage and the type of culverts that were damaged, the longitudinal structural connectivity of the culverts was assumed to be one of the possible reasons for the reported damage mechanism. Therefore, the objective of this paper was to clarify how strongly the longitudinal structural connectivity influenced the longitudinal seismic behavior of the three-hinged arch culverts. To achieve this objective, an elasto-plastic finite element analysis was conducted with an analytical model that could capture the characteristics of the damaged culverts. Simultaneously, a penalty method with the bi-linear spring model was applied as a solution to the contact-impact problems of the precast segmental arch members. As a result, it was found that the weaker longitudinal structural connectivity in the damaged culverts allowed the torsional displacements of the arch members to induce critical damage to the arch members, namely, edge defects in the arch crown and concrete foundation. The numerical results proved the unignorable influence of the longitudinal structural connection on the possible damage to three-hinged arch culverts.


*Keywords:* Three-hinged precast arch culvert; The 2011 off the Pacific Coast of Tohoku Earthquake; Culvert longitudinal direction; Finite element method; Penalty method; Longitudinal structural connectivity

## 1. Introduction

The pre-casting of culvert structures has been incorporated into the recent construction industry trends in Japan to save labor and to optimize earthworks. Many culverts are essentially used as the underpasses of road embankments in order to maintain road linearity in this mountainous country. Ever since the hinge-type precast concrete arch culverts were introduced from France in the middle of the 1990s, they have played an important role in altering cast-in-place culverts. The high quality control of the concrete members by factory production has enabled their rapid construction, and the allowance for arch deformation by the hinge structures has proactively converted the ground reaction to axial stress, which has resulted in the realization of more thinly designed concrete members. A domestic survey of their application along expressways, by Abe and Nakamura (2014), confirmed these advantages with more than 200 examples of construction.

The seismic performance of precast arch culverts is of particular importance in Japan where earthquakes fre-

Peer review under responsibility of The Japanese Geotechnical Society.
* Corresponding author.
*E-mail address:* miyazaki.yusuke.6w@kyoto-u.ac.jp (Y. Miyazaki).

https://doi.org/10.1016/j.sandf.2021.10.005
0038-0806/

quently occur. To the contrary, there were originally few seismic assessments performed in other countries, such as the USA, Canada (e.g., Montgomery et al., 1993; Segrestin and Brockbank, 1995), and countries in Europe. Fig. 1 presents the two representative construction methods used in Japan, namely, the two-hinged type (Association of Modularch Construction Method in Japan, 2017) and the three-hinged type (Technical Committee of Manual for the Design and Construction of Techspan Construction Method in Japan, 1998). Setting aside the differences between them, the two main issues that have been commonly discussed in relation to their seismic design are whether the deformation method built on the seismic studies of underground structures, such as tunnels (e.g., Tamura et al., 1975; Owen and Scholl, 1981; Wang, 1993; Kawashima, 2000), is applicable or not in terms of buried structures in embankments (Byrne et al., 1996; Kumada et al., 1995; Wood and Jenkins, 2000) and how these multi-segmental structures behave in times of earthquakes (e.g., Toyota and Takagai, 1999; Toyota and Ito, 2000). Through not only these seismic studies, but also field measurements with their pre-analyses (e.g., Montgomery et al., 1993; Soba et al., 1997; Sawamura et al., 2019), the structural design of hinged arch culverts has been updated.

However, when the 2011 off the Pacific Coast of Tohoku Earthquake (March 11, 2011) occurred, it caused, for the first time, critical damage such that the three-hinged arch culverts constructed in the early 2000s lost their serviceability (Ojima and Sato, 2011; Abe and Nakamura, 2014). Fig. 2 illustrates the patterns of structural damage, as they were likely to have been caused, namely, continuous flaking of the concrete members occurring on the concrete foundations, flaking of the concrete members at the arch crown, and even on the arch-crown hinges, and deformation of the mouth wall designed by the reinforced earth wall. The drainage plan, foundation ground design, and damage conditions comprehensively placed less emphasis on the causes of either the joint opening of the culvert, correlated with liquefaction in the 2004 Mid Niigata prefecture Earthquake (National Institute for Land and Infrastructure Management (NILM) and Public Works Research Institute (PWRI), 2006) or the embankment collapse, which is suspected to have been caused by the existence of seepage water in both the 2004 Mid Niigata prefecture Earthquake and the 2007 Noto Hanto Earthquake (e.g., Sasaki et al., 2008; Higo et al., 2015). These examples reveal the severity of the damage to the three-hinged arch culvert structures and the imperious necessity for the anti-seismic reinforcing of existing three-hinged arch culverts.

Furthermore, the series of previous studies conducted before and after the 2011 off the Pacific Coast of Tohoku Earthquake do not accurately clarify this damage mechanism. At first, the applicability of the deformation method in the culvert-transverse seismic behavior (see Fig. 1) was confirmed by a physical modeling (Kumada et al., 1995; Toyota and Takagai, 1999) and a numerical analysis (Byrne et al., 1996; Wood and Jenkins, 2000). After the Tohoku Earthquake, Sawamura et al. (2016a, 2017) supported this conclusion up to the ultimate state of the arches by large shaking table tests and reproductive analyses. On the other hand, the culvert-longitudinal seismic behavior was seen to exhibit less seismic integrity between the arches and the surrounding ground in comparison to the culvert-transverse seismic behavior (Kumada et al., 1995; Toyota and Ito, 2000). Miyazaki et al. (2017, 2018) found that the longitudinal structural connectivity controlled the seismic mode of the arches and that a greater overburden of the arches contributed more to the seismic integrity with the arches and the embankment in the longitudinal seismic behavior. These studies indicate the necessity to evaluate the longitudinal seismic performance of the damaged three-hinged arches which might have resulted in the continuous flaking of the arch members due to the lesser seismic integrity of the arches and the embankment.

Accordingly, the aim of the present study was to evaluate the culvert-longitudinal seismic behavior of the three-hinged arches constructed in the early 2000s, especially in terms of their longitudinal structural connectivity. To achieve this objective, the important structural characteristics of the three-hinged arches damaged by the 2011 off the Pacific Coast of Tohoku Earthquake were chosen based on the transition of the structural design of the three-hinged arches. A fully dynamic 3D analysis was implemented with

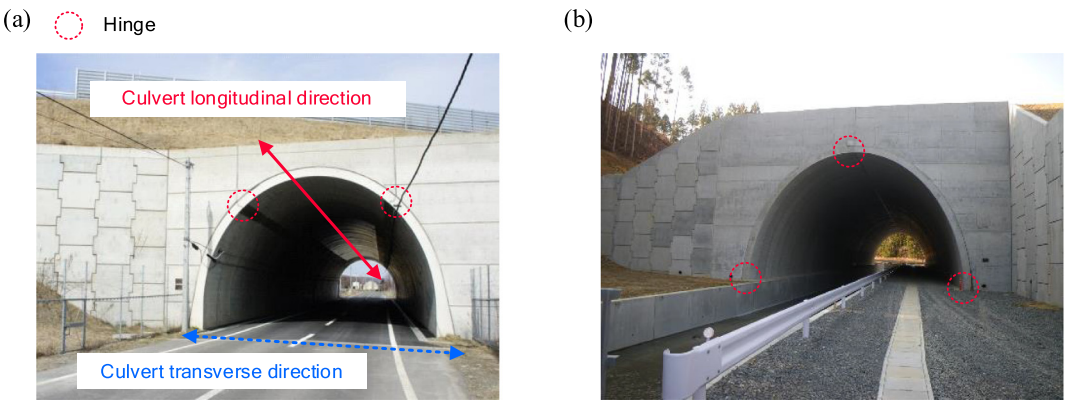


Fig. 1. Hinge types of precast arch culverts: (a) two-hinged arch culvert and (b) three-hinged arch culvert.

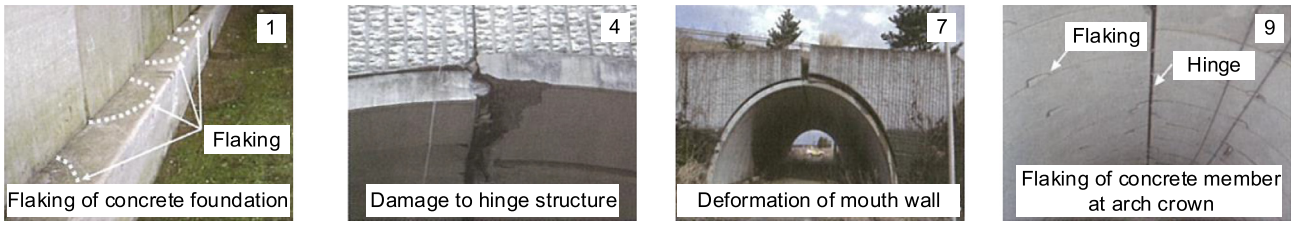


Fig. 2. Reported damage patterns in three-hinged arch culverts constructed in early 2000s (modified after Abe and Nakamura, 2014).

the finite element method which considered the specified and major structural characteristics of the buried three-hinged arch culverts. The major cause of the continuous flaking of the concrete members was considered as a contact-impact problem between the precast segmental arch members. Hence, the penalty method was applied by simply inserting bilinear spring elements between the interfaces of the arch members. In this analysis, the influence of the longitudinal structural connectivity on the culvert-longitudinal seismic behavior was verified by the different longitudinal connected ranges of the arches. Moreover, the deformation of the embankment was considered by an elasto-plastic constitutive model.

## 2. Characteristics of three-hinged arch culverts damaged in 2011 off the Pacific Coast of Tohoku Earthquake

### *2.1. Structural outline of three-hinged arch culvert constructed in early 2000s*

Fig. 3 shows schematic drawings of the structural components of the old type and the current type of three-hinged arch culverts (modified after Seto and Ootani, 2014). Both types are composed of two half-arch members of precast concrete and the foundation (Hutchinson, 2004). They are statically determinate structures due to the three hinges located at the arch crown and arch feet. Three-hinged arch culverts are constructed as follows. Firstly, the casting in place of the concrete foundation, called the 'keyway', is conducted. Then, the two half-arch members are combined so as to bend toward each other and the foundation. Here, a half-depth member is initially arranged to satisfy the staggered arrangement, and grouting is performed at the arch feet of the hinge. Finally, the culverts are filled. When a hinged arch culvert is installed in an embankment, a perpendicular mouth wall is normally constructed for the culvert based on the reinforced soil wall.

Fig. 4 presents schematic drawings of the longitudinal structural connection in the old type of three-hinged arch culvert. Three-hinged arch culverts are constructed by continuously setting the precast RC members at a depth of 1–2 m in the culvert longitudinal direction. Traditionally, the design concept for the culvert longitudinal direction has only considered the prevention of the slipping of the arch members due to the longitudinal gradient of the foundation ground and the uneven settlement. Currently, a concrete

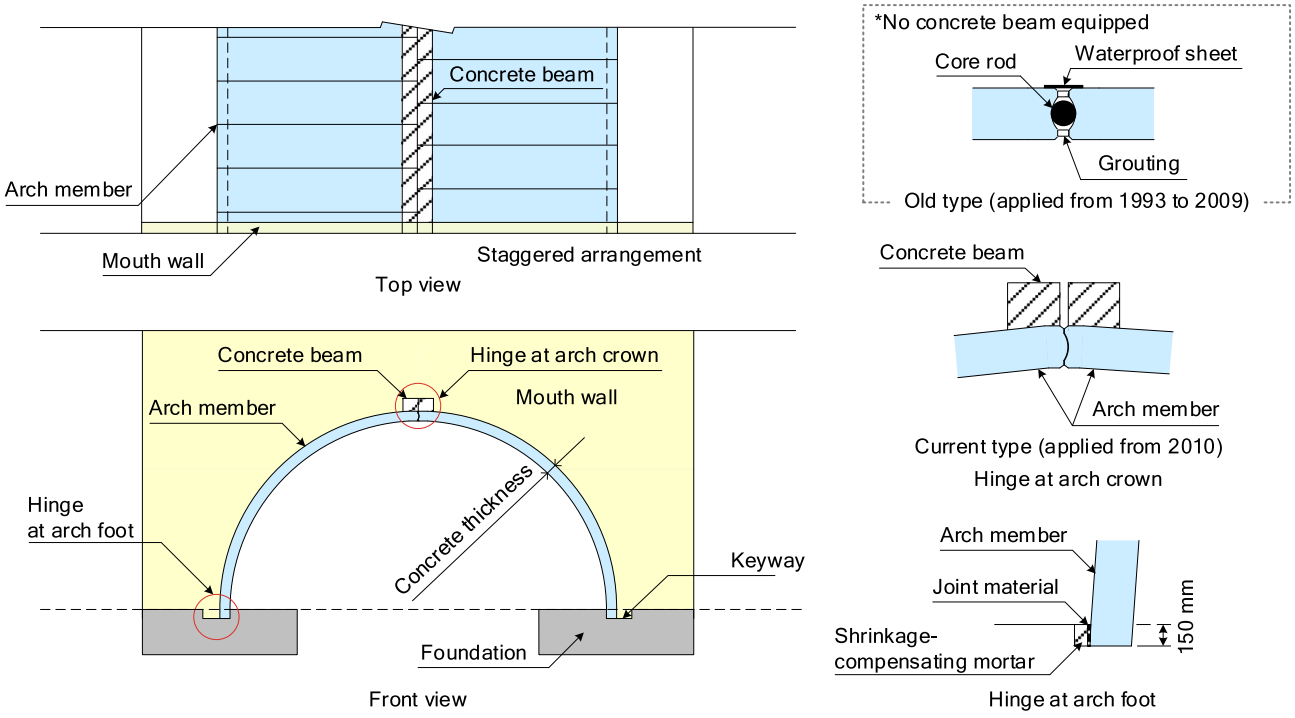


Fig. 3. Schematic drawings of structural components of three-hinged arch culvert (modified after Seto and Ootani, 2014).

beam must be attached at the arch crown (see Fig. 3), for the prevention of longitudinal deformation, as well as at the arch foot, if needed, for the prevention of the overturning of the members.

Examples of the defects of the three-hinged arch culverts, built in the early 1990s in Japan, have triggered the need to update the details in the manual and in the structure. The defects mainly consisted of the slight shift of the old-type hinge structure at the arch crown by longitudinal forces, the inappropriate foundation structure, and the poor and/or degraded embankment material (Public Works Research Institute (PWRI), Nippon Expressway Research Institute Company Limited (NEXCORI) and Graduate School of Engineering, Kyoto University (2020)). Thus, the defects frequently found on the arch crown initiated the main changes in the structural specifications in the longitudinal structural connection starting in 1999 and in the crown-hinge structure starting in 2011 (see Figs. 3 and 4).

### 2.2. Damage characteristics and assumed mechanism

Table 1 shows a profile of the three-hinged arch culverts damaged in the 2011 off the Pacific Coast of Tohoku Earthquake. It is seen from the table that Nos. 2–9 were completed in the early 2000s; their design specifications followed the old-type of structural conditions. Fig. 5 shows the damage situation of No. 9 by an inside observation of the culvert and its assumed damage mechanism by Abe and Nakamura (2014). The drawings in this figure illustrate that edge defects in the arch members of the arch crown occurred overall along the culvert longitudinal direction, while tensile cracks appeared in the arch members located from the mouth of the culvert to the area with a shallow overburden. Moreover, the peeling of the concrete foundation and water infiltration occurred due to the damage to the waterproof sheet for the culverts. In other culverts, the displacement of the hinge of the arch crown (No. 4) and the deformation of the mouth wall (No. 7) occurred (see Fig. 2).

In culvert Nos. 4 and 9, after temporally removing the backfill to observe the damage to the arch crowns, regular patterns of damage were found, as illustrated in Fig. 5(b). For example, damage to the arch crowns continuously occurred along the culvert longitudinal direction on one side of the arch crowns of most arch members due to the separated condition of each arch member. And damage to the concrete foundation continuously occurred along the culvert longitudinal direction on one side of the edge of the arch feet in each of the arch members. In conclusion, as illustrated in the figure, the torsion of the arch members occurred due to the earthquake, knocking the arch members against each other and causing the pattern of damage in them.

The relationship between the locations of the damaged arches and the tectonic deformation by the 2011 off the Pacific Coast of Tohoku Earthquake, as described in Fig. 6 (Geospatial Information Authority of Japan, 2011; Kazama and Noda, 2012), also might indicate a correlation with the contribution to the damage of the culvert-longitudinal seismic behavior. The culverts which suffered damage were constructed along the Joban Expressway; the directions of the extensions of the culverts are seen to be close to the horizontal displacements of the tectonic

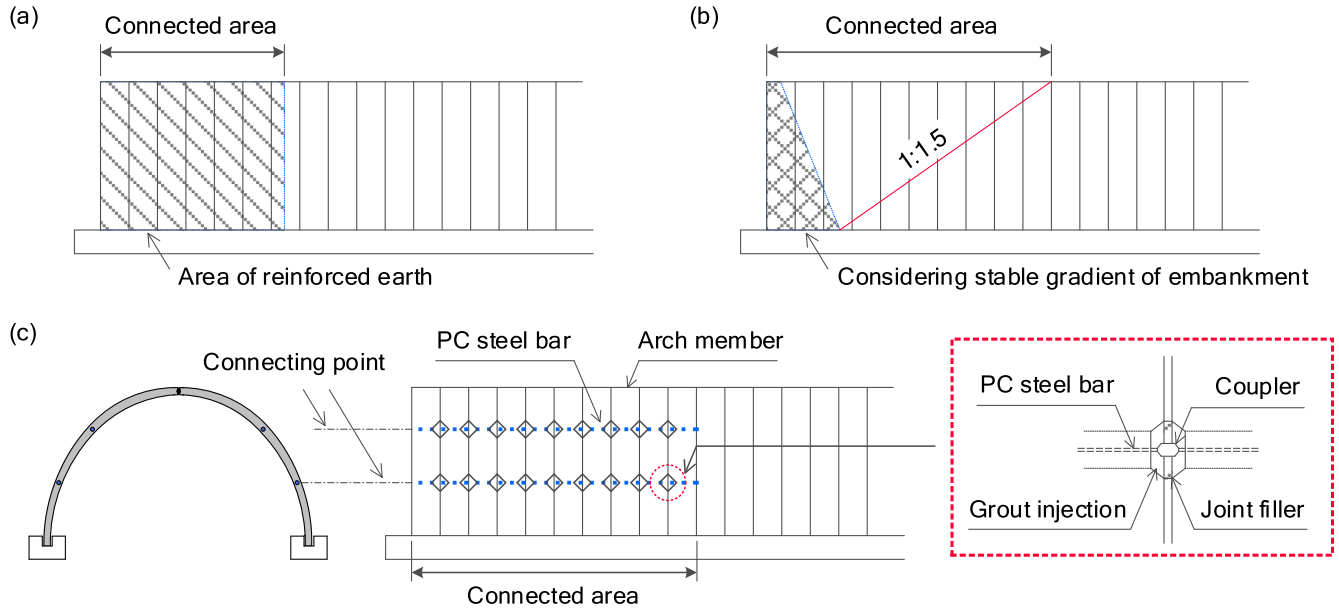


Fig. 4. The longitudinal connection of the arch members depends on the type of hinged arch culvert. In the old type of three-hinged arch culvert, the arch members are (a) connected with the construction of a reinforced earth wall or (b) connected without the construction of a reinforced earth wall, and (c) connected longitudinally by PC steel bars (modified after Technical Committee of Manual for the Design and Construction of Techspan Construction Method in Japan, 1998).

Table 1
Construction profile of three-hinged arch culverts damaged in Great East Japan Earthquake (modified after Abe and Nakamura, 2014).

| No. | Expressway section | $L$ [m] | $f$ [m] | $D$ [m] | $t$ [m] | Filling | Overburden [m] Max. | Overburden [m] Min. | Oblique angle (degree) | Gradient (%) | Type of foundation | Damage level | Completion date |
|---|---|---|---|---|---|---|---|---|---|---|---|---|---|
| 1 | SENDAI-HOKUBU ROAD From RIFU-SHIRAKASHI IC to TOMIYA ICT | 13.2 | 7.3 | 62.4 | 0.35 | Temp. | 13.6 | 1.0 | 90.0 | 1.15 | Continuous | Severe | 2005.1 |
| 2 | Joban Expressway From HIRONO IC to JOBAN-TOMIOKA IC | 5.4 | 2.9 | 64.9 | 0.25 | Temp. | 9.7 | 1.0 | 81.0 | 1.40 | Independent | Minor | 2001.3 |
| 3 | | 9.7 | 5.6 | 39.1 | 0.25 | Temp. | 4.9 | 1.0 | 87.0 | 1.34 | Independent | Severe | 2001.4 |
| 4 | | 9.9 | 5.2 | 46.6 | 0.25 | Temp. | 3.7 | 1.0 | 60.5 | 1.23 | Independent | Severe | 2001.4 |
| 5 | | 10.2 | 5.3 | 45.9 | 0.25 | Temp. | 5.7 | 1.4 | 74.5 | 1.57 | Independent | Small | 2001.12 |
| 6 | | 8.8 | 5.3 | 28.3 | 0.25 | Temp. | 3.2 | 1.0 | 70.0 | 1.20 | Continuous | Severe | 2002.2 |
| 7 | | 7.8 | 4.7 | 30.1 | 0.25 | Temp. | 4.1 | 1.0 | 70.0 | 1.90 | Continuous | Medium | 2002.1 |
| 8 | | 8.2 | 4.7 | 33.4 | 0.25 | Comp. | 2.9 | 1.0 | 90.0 | 2.20 | Independent | Severe | 2002.5 |
| 9 | | 9.0 | 5.3 | 42.8 | 0.25 | Comp. | 2.9 | 1.0 | 90.0 | 0.73 | Continuous | Severe | 2002.9 |

Definition of dimension
$L$ : Inner width of arch culvert.
$f$ : Inner height of arch culvert.
$D$: Longitudinal distance of arch culvert.
$t$ : Thickness of RC arch member.

Definition of damage level
Severe : Most arch members have cracking and peeling.
Medium : A few parts of the arch members have cracking and peeling.
Small : A few parts of the arch members have cracking.
Minor : Arch members have slight cracking.

deformation. Additionally, the staggered arrangement of the half-arch members contributed to this damage pattern, as illustrated in Fig. 5, which also should be considered as an analytical condition.

## 3. Numerical analysis condition

Based on the above discussion, the present analysis was mainly focused on the pure culvert-longitudinal seismic behavior of the buried three-hinged arch culverts varied in their longitudinal structural connectivity and embankment shape. Therefore, the analytical model captured the staggeredly arranged half-arch members of the important structural characteristic of the three-hinged arch culverts. Moreover, the contact-impact problem was considered with the penalty method. Except for these conditions, the minute modeling of the accurate shape of the hinge structure and the reinforced earth wall was simplified as much as possible.

Three-hinged arch culverts are composed of a mouth wall designed by the reinforcing earth wall, the arch members, and the embankment, which requires 3-dimensional modeling for an appropriate damage discussion. That is why the 3D elasto-plastic finite element analysis, operated using a program called DBLEAVES (Ye et al., 2007), was conducted. The applicability of DBLEAVES to ground deformation problems has been verified through various analyses of pile foundations (e.g., Danno and Kimura, 2009) and underground structures, such as tunnels (Cui et al., 2010) and culverts (Sawamura et al., 2015).

Fig. 7 illustrates the assumed deformation mode of culverts installed in an embankment due to the culvert-longitudinal seismic wave and the interfaces and models to produce its deformation with the finite element method. From Fig. 7(a), the longitudinal seismic behavior of the culverts can be explained by the rigid rotation and the sliding of the culverts along with the deformation of the embankment. Therefore, in this FEM analysis, described in Fig. 7(b), the rigid rotation of the culverts was controlled by bilinear spring elements, with the penalty method, arranged at the longitudinal structural connection of the culverts, while the separation and slip were controlled by joint elements arranged at the interface of the culvert and the soil. The embankment deformation was modeled by an elasto-plastic constitutive model.

### 3.1. Analysis mesh and cases

Fig. 8 presents the results of a survey with 127 construction examples of three-hinged arch culverts for road embankments from 1994 to 2014. The damaged arches are seen to be concentrated in areas where the inner width was 10 m and the overburden was 5 m. Here, the extended length is the longitudinal distance of the culverts. The damaged culverts mostly had an extended length of around 20–40 m. This is because precast arch culverts are generally used as the underpasses of road embankments, so that the distance of the culverts was chosen in order to satisfy the available distance for a two-lane road on the embankment crown. In this analysis, considering the calculation cost of the prototype scale, an extended length of 20 m was selected.

Fig. 9 illustrates the analysis meshes based on 20-m-long three-hinged arch culverts on the foundation ground with a thickness of 5.0 m. The slope gradient was adopted from the Guideline for Culvert Work (Japan Road

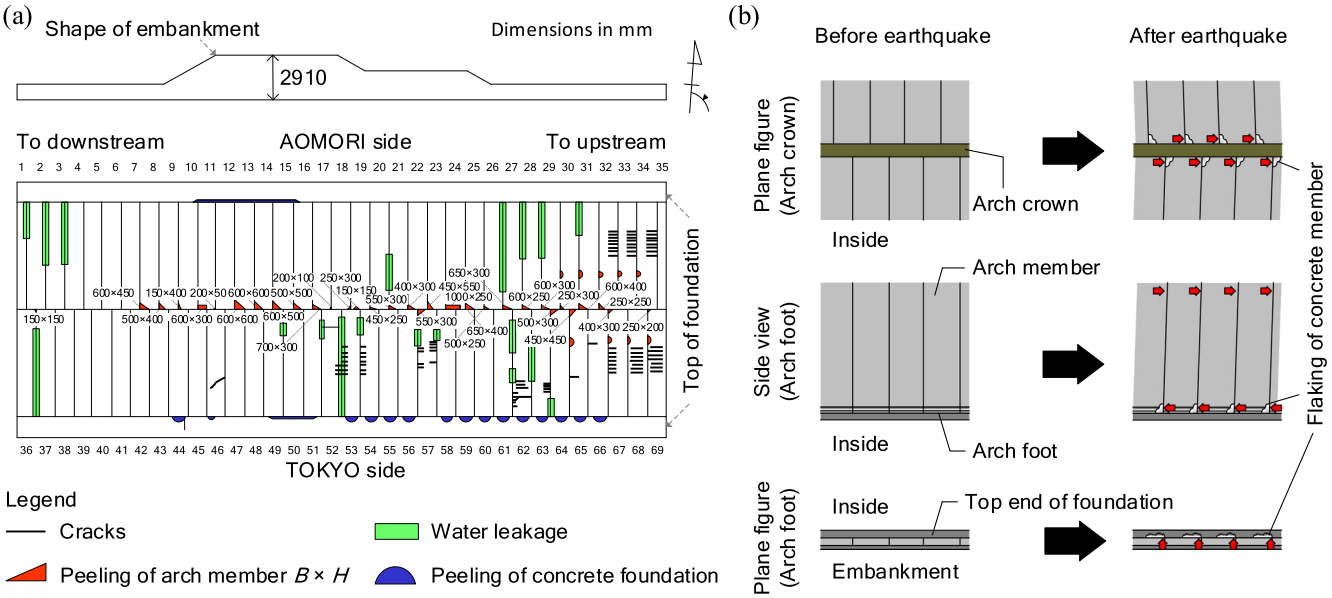


Fig. 5. Schematic drawings of No. 9 (a): damage situation and (b) assumed damage mechanism of arch members during earthquake (modified after Abe and Nakamura, 2014).

Association, 2010). The hinge of the arch crown was in a simply butted condition instead of modeling the mechanical function of the hinge by spring elements. The mouth wall considered the actual segmental condition (see Figs. 2 and 9). The perpendicular wall elements and the embankment elements are continuous with the joint element arranged at the interface between them. The present analysis did not consider the reinforcement of the mouth wall due to the difficulty of creating an accurate modeling of the arrangements of the reinforcements and their frictional behavior with the embankment. The unity of the reinforced earth wall and the hinged arch culverts was confirmed through dynamic centrifuge model tests (Miyazaki et al., 2017, 2018). In this case, the mouth wall model may possibly lose its unity with the embankment because consideration was not given to the effect of the reinforcing member in the backfill. Therefore, a certain magnitude of input wave, as will be described later, was chosen so as not to cause the separation of the mouth wall from the embankment.

Table 2 summarizes the eight analytical cases based on the considered conditions. The patterns of the maximum overburden, used to discuss its effect, are 1.0 m as H-1 and 5.0 m as H-5; they correspond to the names of the analytical cases. As for the influence of the longitudinal struc-

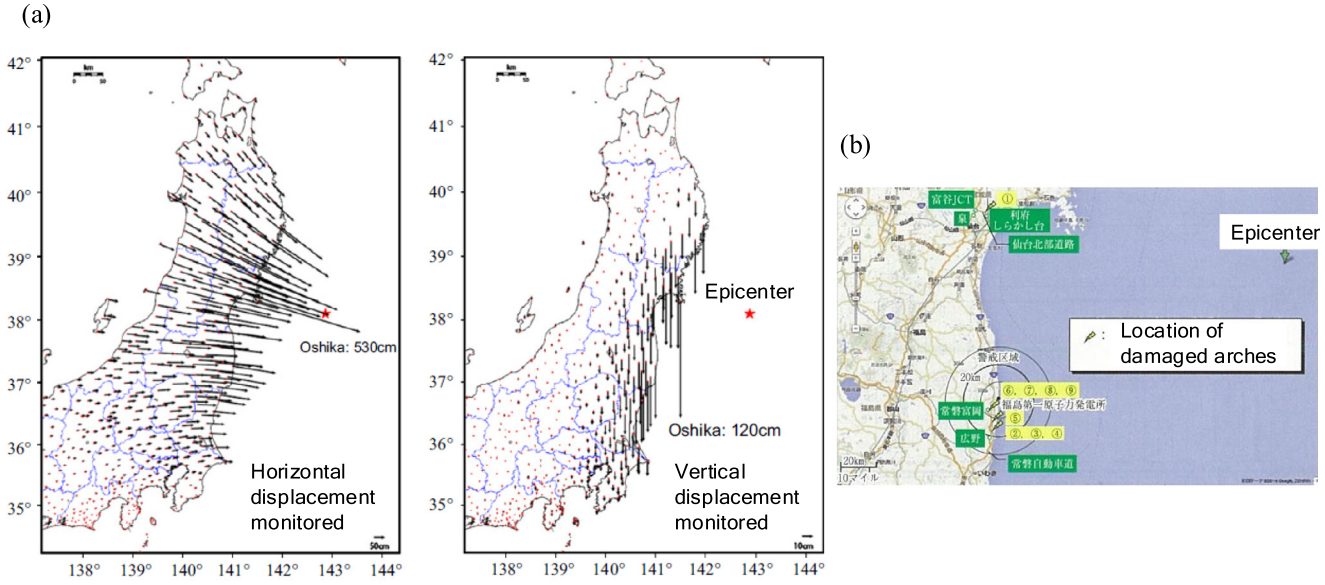


Fig. 6. Relationship between (a) tectonic deformation by main earthquake on March 11 (Kazama and Noda, 2012 and document published by GSI, 2011), 2011 and (b) location of damaged precast arch culverts (modified after Abe and Nakamura, 2014).

tural connectivity, the range in the connected area varied with longitudinal connecting intensity *LCI*, as follows:

$$LCI = L_c/L_e \quad (1)$$

Here, $L_c$ is the longitudinal length of the longitudinally connected arches, counted from both mouths of the culvert (see Table 2) [m], and $L_e$ is the extension length of the arch culvert. $L_e$ constantly equals 20.0 m. It should be noted that the longitudinal connection normally starts from the mouth of the culvert as the longitudinally connecting direction of *LCI* also follows. *LCI* was simply varied in four patterns: 0 ($L_c = 0$), 0.25 ($L_c = 5.0$), 0.5 ($L_c = 10$), and 1.0 ($L_c = 20$), with '$LCI = 0$' meaning that no arches were longitudinally connected.

### 3.2. Interface of arch members

The solutions for contact-impact problems using a grid scheme and a particle method, such as the finite element method and the moving particle simulation, are based on Lagrange's method of undetermined multipliers (Hughes et al., 1976) or the penalty method (e.g., Suzuki and Toi, 1987). In particular, the penalty method is equivalent to inserting a spring element into each of the contact points. Therefore, the implementation of the simulation is relatively simple, although there is a problem of vibrations in the structure at higher order modes (Suzuki and Toi, 1987). However, the present study attempted to express the separated connection of each arch member with a simple physical meaning. In this numerical analysis, a bilinear spring element is inserted into each contact node of the culvert elements along with the use of the original penalty method.

Fig. 10 describes the interfaces of each arch element and soil element for the contact-impact problem and soil-structure interaction. The arch members were modeled as an elastic material whose mechanical properties were based on concrete, as shown in Table 3. The joint elements were arranged on the interface between the arch culvert and the soil for modeling the slip and separation. The interface of the culverts and the soil has joint elements whose parameters were determined by direct shear tests between mortar and Toyoura sand (Sawamura et al., 2016b). Table 4 shows the material properties of the joint elements. It should be noted that the shear stiffness of the joint elements between the mouth wall and the embankment was set to have the same value as the joint elements between the culvert and the soil. The bilinear spring elements were arranged in the longitudinal structural connection of the arch members. The hinge of the arch crown was modeled with the bilinear spring elements between the elements of the arch crown, and the hinges of the arch feet were modeled with joint elements between the elements of the arch feet and the foundation.

Fig. 11 shows the stiffness laws for the bilinear spring elements. In this analysis, to express the openings of the three-hinged arches reported after the 2011 off the Pacific Coast of Tohoku Earthquake, the spring elements were controlled to have tensile stiffness equal to zero under the contactless condition and stiffness that was sufficiently larger than concrete at the contacts. The hinge at the arch crown was modeled by considering the friction of the concrete (Kono et al., 2013); the rotating stiffness was quite small. The hinges at the arch feet were modeled by joint elements, as shown in Fig. 10(a).

### 3.3. Constitutive model for ground

The present study used the cyclic mobility model proposed by Zhang et al. (2007) for the constitutive model of the banking soil. Their model was developed to describe the cyclic mobility of soil by systematically combining the evolution equations for the development of stress-induced anisotropy and the changes in the over-consolidation of the soil. As an important advantage, the proposed model can express the behavior of soil under cyclic loading with different drained conditions and by uniformly considering the density, over-consolidation ratio, naturally accumulated structure of the soil, and stress-induced anisotropy of the soil.

In this paper, a simple introduction of the normal yielding surface of the cyclic mobility model is given. Here, based on the research work by Asaoka et al. (2002), the similarity ratio of the superloading surface to normal yield

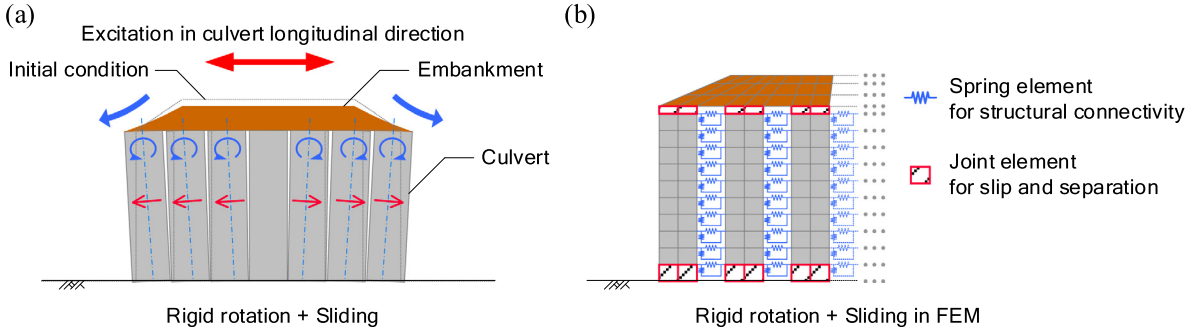


Fig. 7. Deformation mode of culverts due to seismic wave in culvert longitudinal direction: (a) observed deformation mode in experiment and (b) modeling by finite element method.

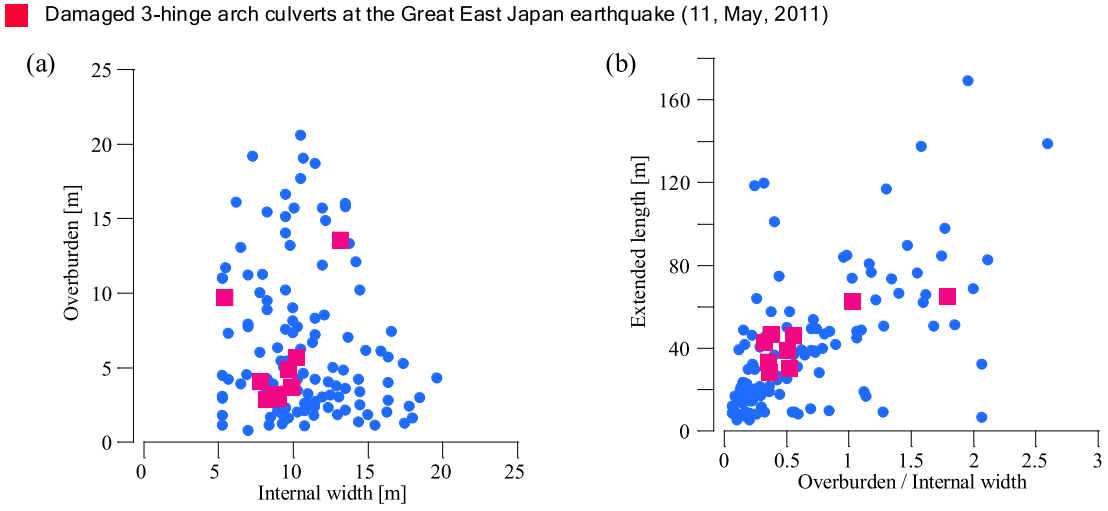


Fig. 8. Analysis of construction examples of three-hinged arch culverts based on open resource of construction classifications Hokyodo net service, 2014; classifications: (a) by internal width and overburden and (b) by overburden ratio (overburden/internal width) and extended length.

surface $R^*$ and the similarity ratio of the superloading surface to subloading surface $R$ are the same, namely,

$$R^* = \frac{\tilde{p}}{\bar{p}} = \frac{\tilde{q}}{\bar{q}}, \quad 0 < R^* \leqslant 1 \tag{2}$$

$$R = \frac{p}{\bar{p}} = \frac{q}{\bar{q}}, \quad 0 < R \leqslant 1, \quad R = \frac{1}{OCR} \tag{3}$$

$$\frac{\bar{q}}{\bar{p}} = \frac{\tilde{q}}{\tilde{p}} = \frac{q}{p} \tag{4}$$

where $(p', q)$, $(p', q)$, and $(\bar{p}', \bar{q})$ represent the present stress state, the corresponding normally consolidated state, and the structured stress state at the $p$-$q$ plane, respectively.

Therefore, according to Fig. 12, normal yield surface $R^*$ is given in the following equations:

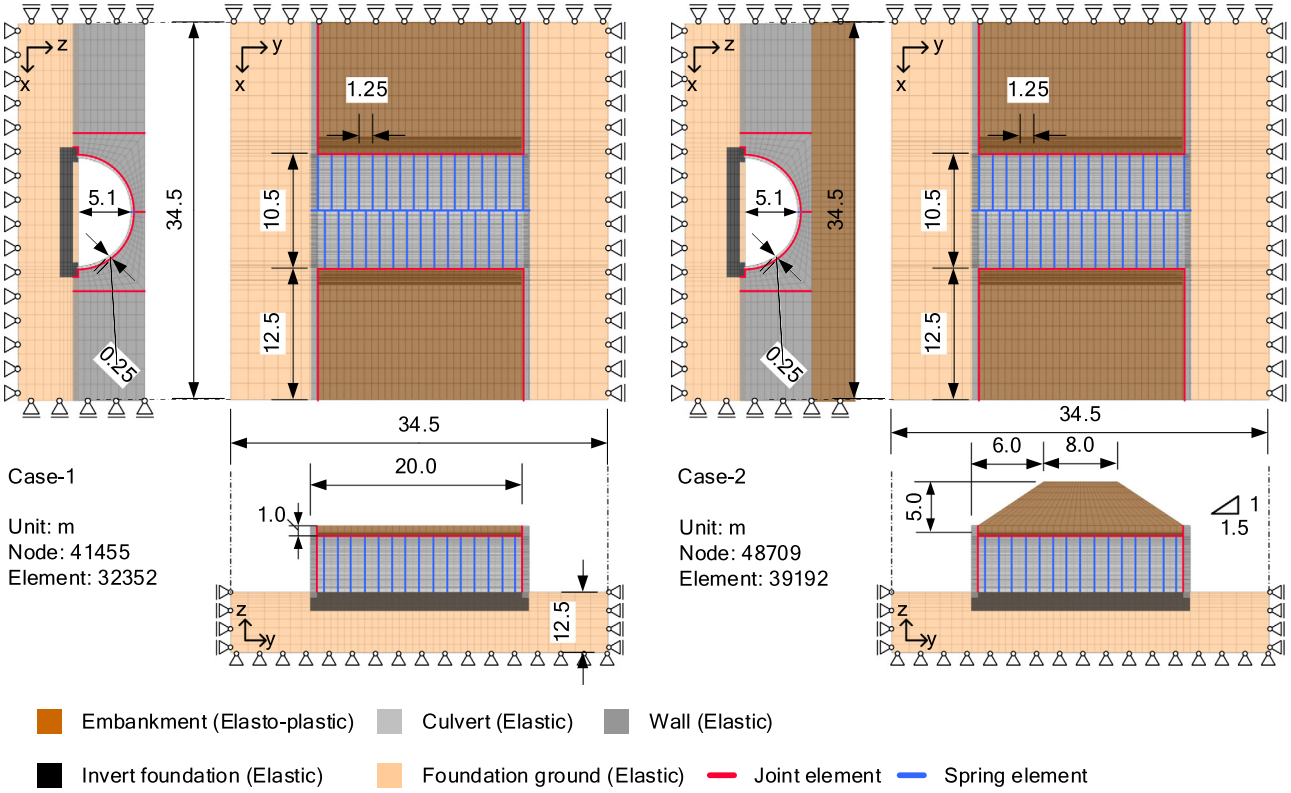


Fig. 9. Analysis meshes in Case-1 and Case-2.

Table 2
Analysis cases.

| Maximum overburden [m] | *LCI* [m/m] | | | |
|---|---|---|---|---|
| | 0 | 0.25 | 0.5 | 1.0 |
| 1.0 | Case-1_0 | Case-1_0.25 | Case-1_0.5 | Case-1_1.0 |
| 5.0 | Case-2_0 | Case-2_0.25 | Case-2_0.5 | Case-2_1.0 |

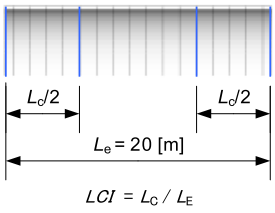


*The present analysis models 33 precast arch segmental members. The right-hand side of the arch culverts, shown in Fig. 9, composes 16 arch members, while the left-hand side of the arch culverts composes 17 (15 full-depth arch members and 2 half-depth arch members for a staggered arrangement). For simplification, the connecting intensity is calculated with the number of longitudinally connected arch members arranged at the right-hand side of the culverts where only full-depth arch members are constructed (e.g., 0.25 = 4 longitudinal connected arch members / 16 arch members).

$$f = \ln\frac{\tilde{p}}{p} + \ln\frac{M^2 - \varsigma^2 + \eta^{*2}}{M^2 - \zeta^2} - \frac{\varepsilon_v^p}{C_p} = 0 \tag{5}$$

$$\eta^* = \sqrt{\frac{3}{2}\hat{\eta}_{ij}\hat{\eta}_{ij}},\ \hat{\eta}_{ij} = \eta_{ij} - \beta_{ij},\ \eta_{ij} = \frac{S_{ij}}{p},\ S_{ij} = \sigma_{ij} - p\cdot\delta_{ij},\ p = \frac{\sigma_{ij}}{3} \tag{6}$$

$$\eta = \sqrt{\frac{3}{2}\eta_{ij}\eta_{ij}},\ \varsigma = \sqrt{\frac{3}{2}\beta_{ij}\beta_{ij}} \tag{7}$$

$$C_p = \frac{\lambda - \kappa}{1 + e_0} \tag{8}$$

where $S_{ij}$ is the deviatoric stress tensor and $\beta_{ij}$ is the anisotropic stress tensor.

The cyclic mobility model requires eight parameters. Five of the eight parameters are equivalent to those of the Cam-clay model (*Rcs, λ, κ, N* and $v_e$), which can be determined by triaxial compression tests. The other three parameters (*a, m,* and $b_r$) require trial and error of the fitting of the results obtained from the triaxial tests. The respective physical meanings of the parameters are clear. The parameters were determined by triaxial tests and isotropic consolidation tests on Edosaki sand (Fig. 13, Sawamura et al., 2016b). Based on the simulation results, the parameters for the cyclic mobility model and the state variables of $R^*0$ and ζ0 were determined as shown in Table 5.

The foundation ground was modeled by an elastic model whose stiffness had a value of 30 *N* for the SPT. This is because the three-hinged arch culverts require specified ground conditions, including a value of more than 30 *N* for the SPT in the foundation ground (Technical Committee of Manual for the Design and Construction of Techspan Construction Method in Japan, 1998). Moreover, the damage to the three-hinged arches, reported after the 2011 off the Pacific Coast of Tohoku Earthquake, had no clear correlation with the deformation of the foundation ground. That is why, in the present analysis, the plastic deformation of the foundation ground was not considered. The Young's modulus of the foundation ground was calculated by 2800 *N* = 84,000 k Pa based on the empirical formula suggested by the Japan Road Association (2012).

The initial stress of the foundation ground and the culverts was determined through a self-weight analysis, while the initial stress of the embankment was determined as the $K_0$ state of the soil, considering the stability of the calculation. The earth pressure coefficient was calculated with Jaky's formula and the internal friction angle of the Edosaki sand.

### 3.4. Input wave

For the input wave in the culvert longitudinal direction, a sinus wave with 1 Hz, three cycles, and 300 Gal of magnitude (Fig. 14) was used to observe the simple seismic behavior. To clarify the fundamental influence of the longitudinal structural connectivity, a simple but strong frequency of the recorded earthquakes (Japan Road Association (JRA), 2012) was selected. The wave was input at the bottom of the foundation ground in the culvert longitudinal direction as a fundamental investigation of the seismic behavior of the old type of three-hinged arch culverts. The time interval of the calculation was 0.001 s, and the time integration was based on the Newmark-$\beta$ method ($\beta$ = 1/4 and $\gamma$ = 1/2).

## 4. Analysis results

Compressive displacements and loads are positive in the following analysis results. The displacement and loads of the longitudinal structural connection were obtained from the spring elements in the Y-axis direction arranged between each longitudinal section of arch members (see Figs. 9 and 10). Here, the tensile displacements physically match the openings between each arch member. Fig. 15 illustrates the coordinates in the analysis mesh. The heatmap of the stress follows this coordinate rule.

### 4.1. Displacements and loads on longitudinal structural connection

The magnitude of the tensile force required to induce the joint openings between each arch member is supposed to highly depend on the longitudinal position of the arch

member. This is not only because the deformation of the surrounding ground is likely to induce the joint openings of each arch member, but because the ground deformation also varies depending on the different deformation of the arches due to their longitudinal structural connection. Therefore, the maximum tensile displacement and force were chosen for each jointed section of the arch members and are summarized in Fig. 16.

Fig. 16(a) shows the normalized values for the maximum displacements at each longitudinal structural connection during excitation. The values were normalized by the maximum displacement in the all longitudinally non-connected condition of Case-1 (Case-1_0), −14.45 mm. From the figure, in both overburden conditions of 1.0 m and 5.0 m, if the arches are partially, longitudinally connected, the tensile displacements tend to be maximized at the first longitudinal separation. In the all longitudinally non-connected arches, Case-1 exhibits the largest tensile displacements of any of the longitudinal conditions. However, in Case-2, the largest tensile displacement was observed in Case-2_0.5 which is the partially connected condition. Additionally, focusing on the overburden condition, Case-1 shows larger tensile displacement than Case-2 under any longitudinal connecting conditions. These results indicate the following two possibilities under the input wave of 1 Hz; the openings of the longitudinal joints between each arch member are enlarged by a smaller overburden, and the largest opening between joints due to the longitudinal excitation varies with the combination of the overburden and the range in the longitudinal structural connection.

Fig. 16(b) exhibits the normalized maximum tensile loads during excitation at each longitudinal structural connection. To normalize these tensile loads, the largest tensile value in the all longitudinally connected condition in Case-1 (Case-1_1.0) of −129.15 kN was used. It is seen from the figure that, if the arches are partially, longitudinally connected, the maximum tensile loads acting on the longitudinal structural connection will be greatly decreased, namely, about 30% of the largest tensile load obtained in Case-1_1.0. And in comparing Case-1_1.0 and Case-2_1.0, in the all longitudinally connected condition, the tensile loads reach larger values with an increase in the overburden. On the other hand, with an increase in the longitudinal connection, the maximum tensile loads tend to be closer to the distribution of tensile loads in the all connected condition.

Table 3
Material properties of concrete culvert model.

| | | | |
|---|---|---|---|
| *Young's* modulus | $E_e$ | [kN/m$^2$] | $3.10 \times 10^7$ |
| Unit weight | $\gamma$ | [kN/m$^3$] | 24.5 |
| Poisson's ratio | $v$ | – | 0.20 |
| Damping ratio | $h$ | – | 0.02 |

Table 4
Material properties of joint elements.

| | | | |
|---|---|---|---|
| Shear stiffness | $K_s$ | [kN/m$^2$] | $1.55 \times 10^5$ |
| Normal stiffness | $K_n$ | [kN/m$^3$] | $1.55 \times 10^5$ |
| Cohesion | $c$ | – | 5.00 |
| Internal friction angle | $\phi$ | – | 28.0 |

The seismic behavior in the longitudinal structural connections is summarized in Fig. 17. In Fig. 17(a), the longitudinal displacements of the arch section are described. This figure illustrates the tensile displacements at the longitudinal connection whose maximum tensile displacements are observed in Fig. 16(a). From the figure, the tensile displacements are seen to be maximized near the arch crown in both Case-1 and Case-2. Fig. 17(b) exhibits the time histories of the longitudinal displacements of the nodes where the maximum tensile displacements are observed. In the figure, the tensile displacements in all cases are seen to be amplified during excitation and to reach the constant rest value after excitation. The longitudinal connective displacements might be brittle due to the deformation of the embankment. Based on these analysis results, the way in which these dynamic behaviors of the longitudinal connections resulted in the deformation and stress of the arches and the mouth wall is discussed.

### 4.2. Stress and deformation of arch members and mouth wall after excitation

Fig. 18 presents heatmaps of the embankment, including the culvert and the mouth wall, of the normalized displace-

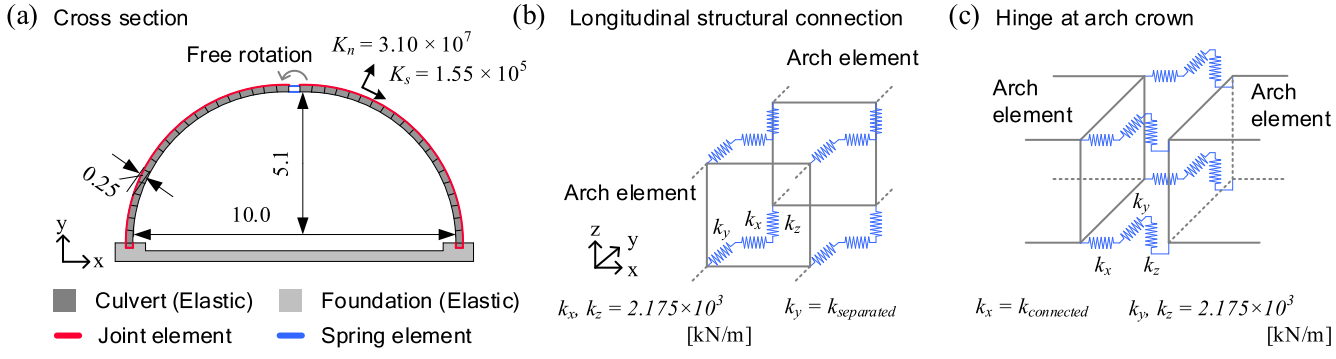


Fig. 10. Soil-structure interface and structure-structure interface of arch elements.

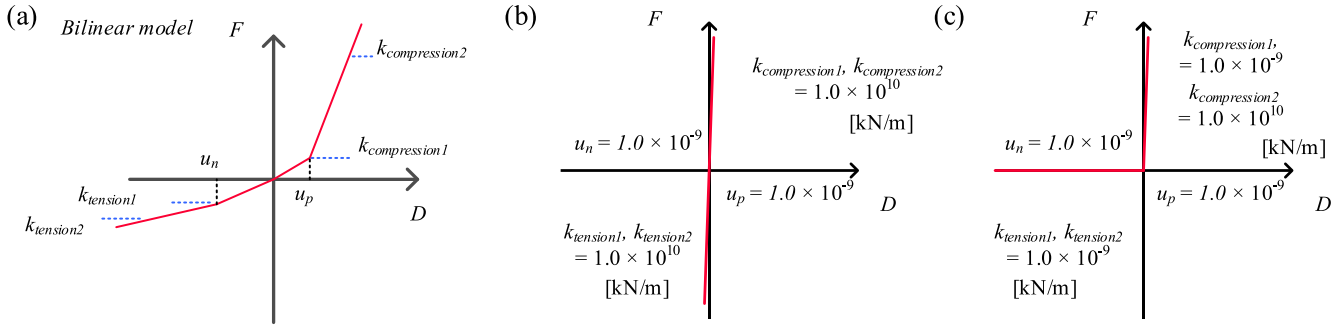


Fig. 11. Spring model for contact-impact of culvert elements: (a) bilinear model of spring element, (b) spring constant in connected condition, and (c) spring constant in separated condition.

ments in the Y-axis direction. The values are normalized by the maximum displacements in the all longitudinally separated condition for Case-1 and Case-2. From the figure, the displacements are seen to be maximized in all cases in positive and negative directions at the mouth wall of the culverts. Under the input wave of 1 Hz, 300 Gal, and three cycles of sinus waves in the longitudinal direction, the deformation of the mouth wall is enlarged at the area of the culvert's installation. The displacement of the mouth wall might be controlled by the dynamic behavior of the arch members. Thus, focus is placed on the deformation and stress state of the arch members and the mouth wall in this order.

Fig. 19 shows heatmaps of the normalized $\tau_{xy}$ shear stress of the arch members after excitation. The figure is illustrated from the viewpoint of the XY-plane. The shear stress is normalized by each maximum $\tau_{xy}$ in Case-1 and Case-2. In the figure, focus is placed on the deformation of the arches, if the arches are partially, longitudinally connected. In all cases, the openings of the arch members tend to be enlarged at the first longitudinally non-connected section. In other words, the openings of the arch members occur toward the mouth of the culvert, which can capture the deformation mode of the longitudinally separated precast arches after the repeated shaking in the culvert longitudinal direction (Miyazaki et al., 2017). Examining the stress state of the arches, Case-1_1.0 shows the largest shear stress in Case-1 mainly due to the concentration of stress at the mouth of the culvert. On the other hand, Case-2_1.0 does not show the same tendency. Even though a higher concentration of stress is observed in Case-2_1.0, the whole stress level of the arches remains higher in the other cases. Surely the increase in overburden amplifies the shear stress level compared with Case-1 and Case-2. Therefore, due to the overburden or the embankment shape, the respective arch members might have larger shear stress in the all longitudinally separated and partially, longitudinally connected conditions than those in the all longitudinally connected condition.

Fig. 20 illustrates heatmaps of the normalized displacements in the Y-axis direction and the $\tau_{yz}$ of the mouth wall after excitation. To normalize each value, the maximum values in Case-1_0 and Case-2_0 are used. It is seen from the figure that, in all cases, with the increase in the connecting intensity, the displacements in the Y-axis direction are decreased. The $\tau_{yz}$ of the mouth wall is coincident with the direction of the mouth wall inclining forward and is maximized near the arch feet. These results indicate that the displacements of the mouth wall were generated purely by the displacements of the arch members because the upper area of the mouth wall near the arch crown exhibited little shear stress in the YZ-plane.

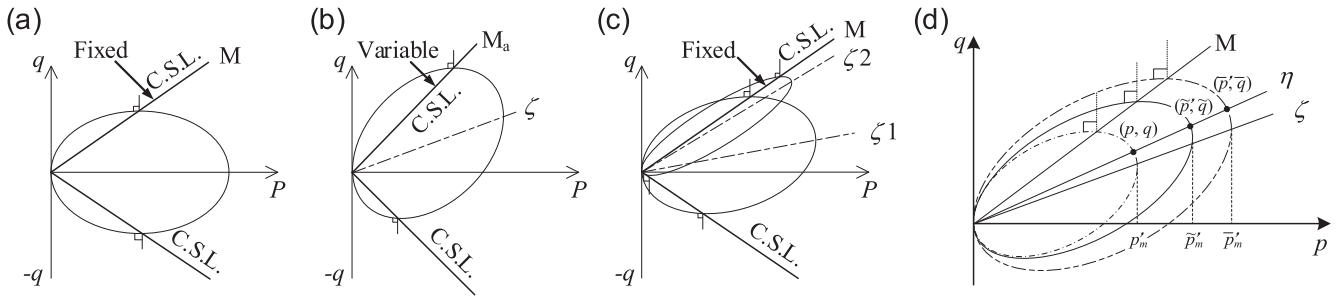


Fig. 12. Concept of yielding surfaces in cyclic mobility model (Zhang et al., 2007): changes in subloading yielding surfaces at different anisotropy ζ in (a) modified Cam-clay model (Schofield and Wroth, 1968), (b) SYS Cam-clay model (Asaoka et al., 2002), (c) cyclic mobility model, and (d) subloading, normal, and superloading yield surfaces in *p*-*q* plane adopted in cyclic mobility model.

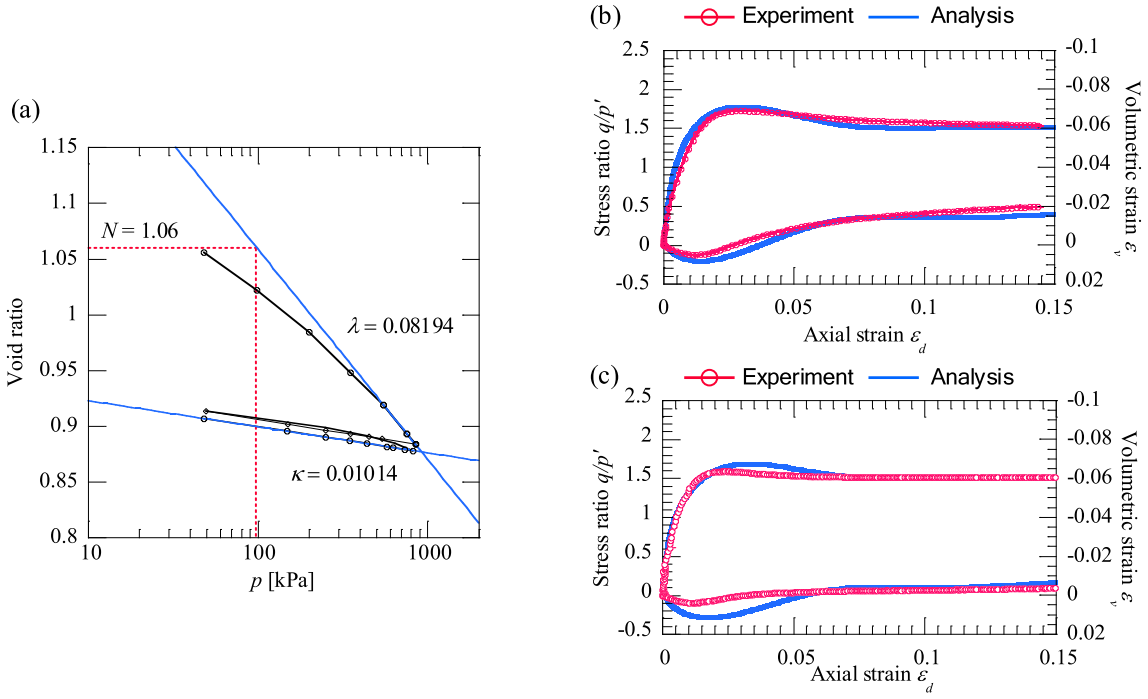


Fig. 13. Results of (a) isotropic consolidation tests and triaxial compression tests and their simulation in (b) 50 kPa of confining stress, and (c) 100 kPa of confining stress for Edosaki sand (Sawamura et al., 2016b).

## 5. Discussions

### 5.1. Quantitative evaluation of seismic effect of longitudinal structural connectivity

As exhibited above, the previous analytical results from the 3D elasto-plastic dynamic analysis prove the unignorable influence of the longitudinal structural connection on the possible damage to three-hinged arch culverts. To summarize these seismic effects, the connecting intensity is used as an evaluation index to confirm the dynamic behavior of the longitudinal structural connection and the rest deformation and stress of the arches and the mouth wall as their results. Fig. 21 illustrates the maximum values of the displacements and the forces on the longitudinal structural connection during excitation, and the maximum displacements in the Y-axis direction of the mouth wall and the maximum $\tau_{xy}$ of the arches after excitation.

From the figure, focused on the longitudinal structural connection, the increase in the connecting intensity is seen to be coincident with the increase in the maximum tensile

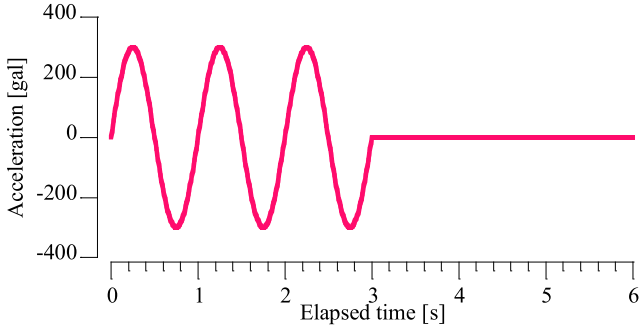


Fig. 14. Input wave: sinus wave with 1 Hz and three cycles with magnitude of 300 Gal.

Table 5
Parameters for cyclic mobility model.

| | |
|---|---|
| Principal stress ratio at critical state $R_{CS} = (\sigma_1/\sigma_3)_{CS(comp.)}$ | 4.0 |
| Compression index $\lambda$ | 0.082 |
| Swelling index $\kappa$ | 0.101 |
| $N = e_{NC}$ at $p = 98$ kPa & $q = 0$ kPa | 1.06 |
| Poisson's ratio $\nu_e$ | 0.276 |
| Degradation parameter of overconsolidation state $m$ | 0.020 |
| Degradation parameter of structure $a$ | 0.65 |
| Evolution parameter of anisotropy $b_r$ | 0.4 |
| Wet unit weight (kN/m$^3$) $\gamma_t$ | 17.738 |
| Initial degree of structure $R^*_0$ | 0.1491–0.1584 |
| Initial anisotropy $\zeta_0$ | 0.5 |

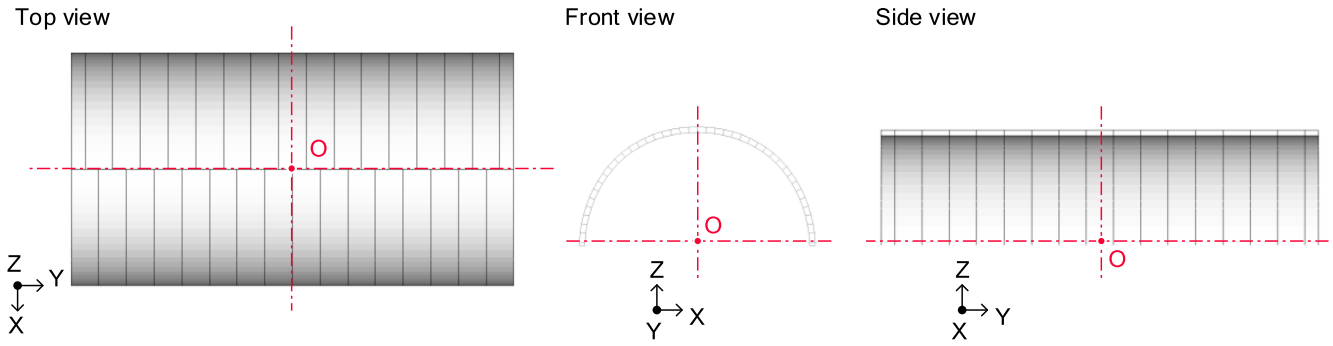


Fig. 15. Origin of coordinates in present analysis.

force of the longitudinal structural connection, although it is not coincident with the tensile displacements. On the other hand, focused on the mouth wall and the arches, the maximum displacement in the Y-axis direction of the mouth wall is seen to be suppressed linearly with the increase in the connecting intensity, and the maximum $\tau_{xy}$ of the arches does not linearly follow the increase in the connecting intensity. In short, according to the overburden or the embankment shape condition, an appropriate longitudinal connected range exists for decreasing the openings of the arches or the cross-sectional force on the arches.

Fig. 22 presents the total scores of the normalized values shown in Fig. 21. With the figure, the total influence of the connecting intensity on the plotted physical values in Fig. 21 can be discussed. The appropriate longitudinal connection should be designed in accordance with the order of priority in the required performance of the three-hinged arches. For example, with a small overburden pattern, like that in Case-1, the dynamic behavior of the whole culverts is strongly affected by the arches so that all precast segmental arches should be longitudinally connected. Considering the smallest total score obtained in the connecting intensity of 1.0 in Case-1, this

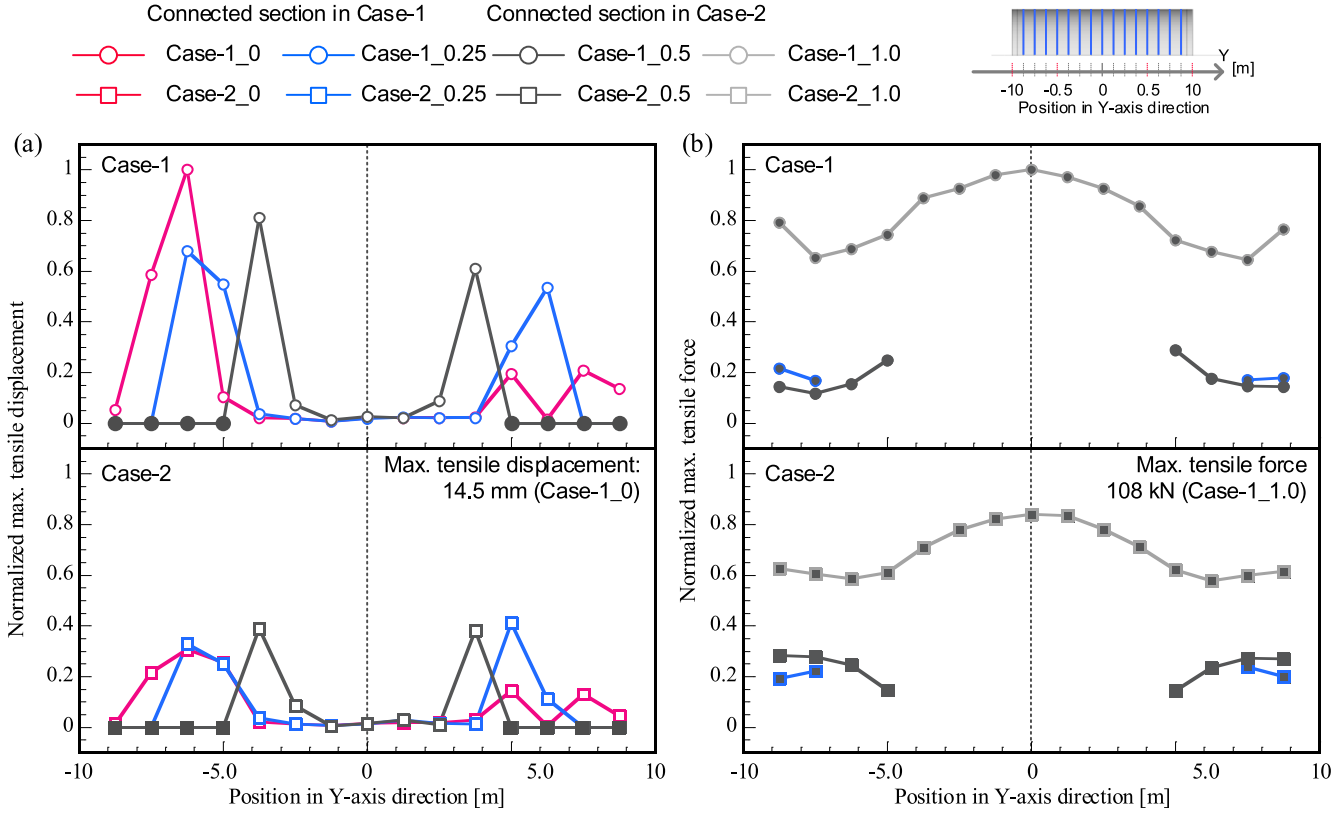


Fig. 16. Normalized maximum tensile displacements of longitudinal connection during excitation in (a) Case-1 and (b) Case-2. The open markers stand for the longitudinally separated sections and the solid markers stand for the longitudinally connected sections.

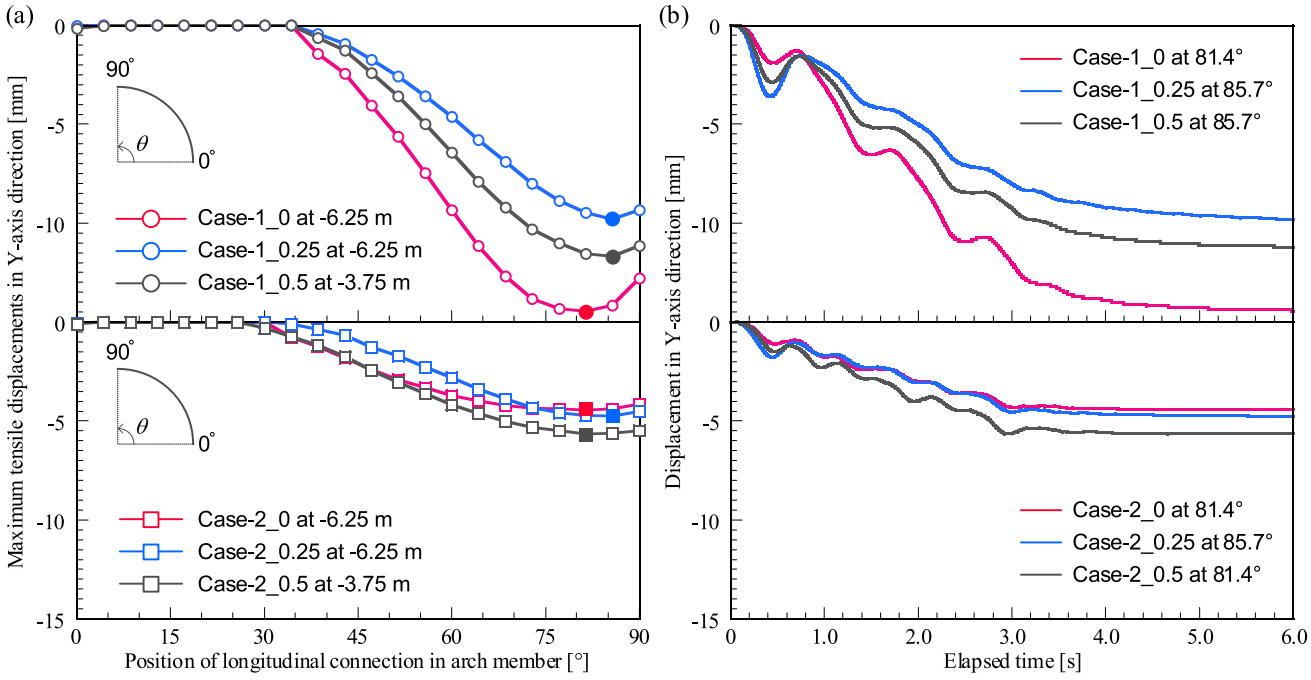


Fig. 17. Evaluations of (a) displacements of joints of arch members where largest tensile displacement occurred during excitation and (b) time histories of displacements in Y-axis direction of composed nodes where largest tensile displacements occurred in joints between arch members.

recommendation can be supported. On the other hand, balancing the total score, the stress level of the arches, and the number of longitudinally connected sections, the connecting intensity of 0.5 is recommended especially with a larger overburden, like that in Case-2. It should be noted that the discussions are based on the input wave with a sinus wave of 1 Hz, for simplicity, considering the research objective, and that the longitudinal dynamic behavior of various frequencies and phases should be considered in future studies.

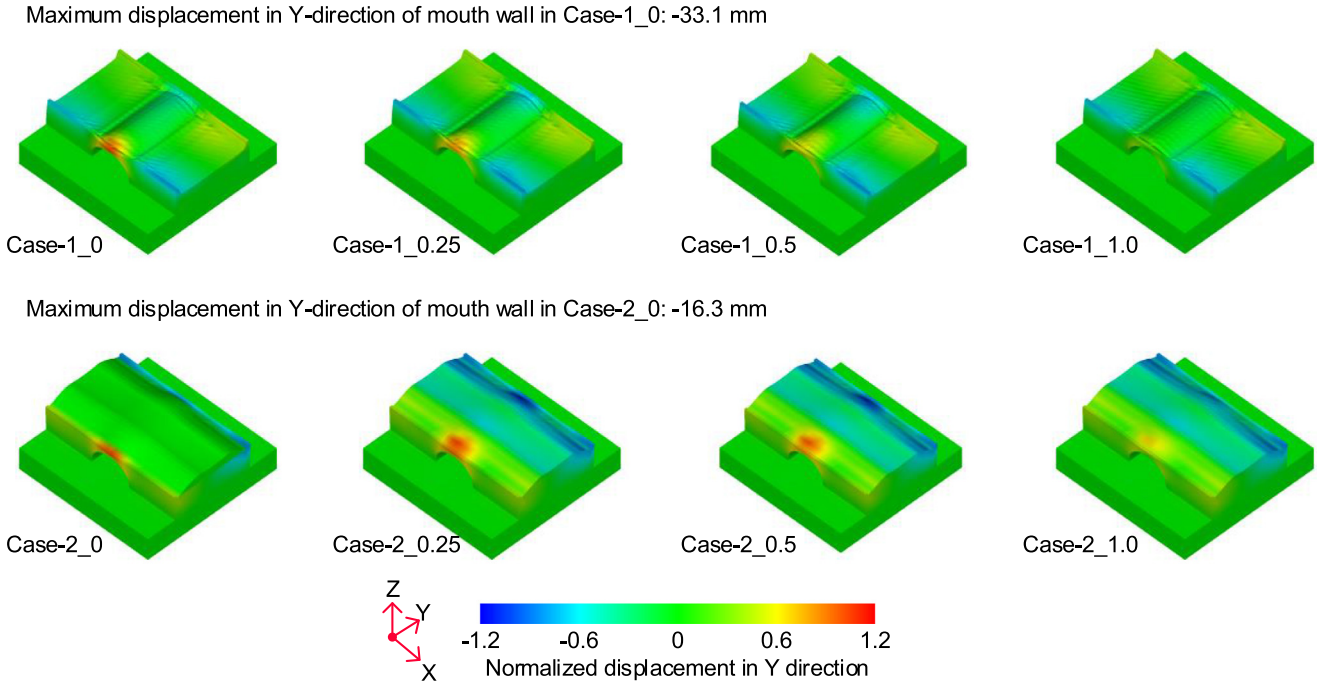


Fig. 18. Heatmaps of normalized displacement in Y-axis direction after excitation in Case-1 and Case-2.

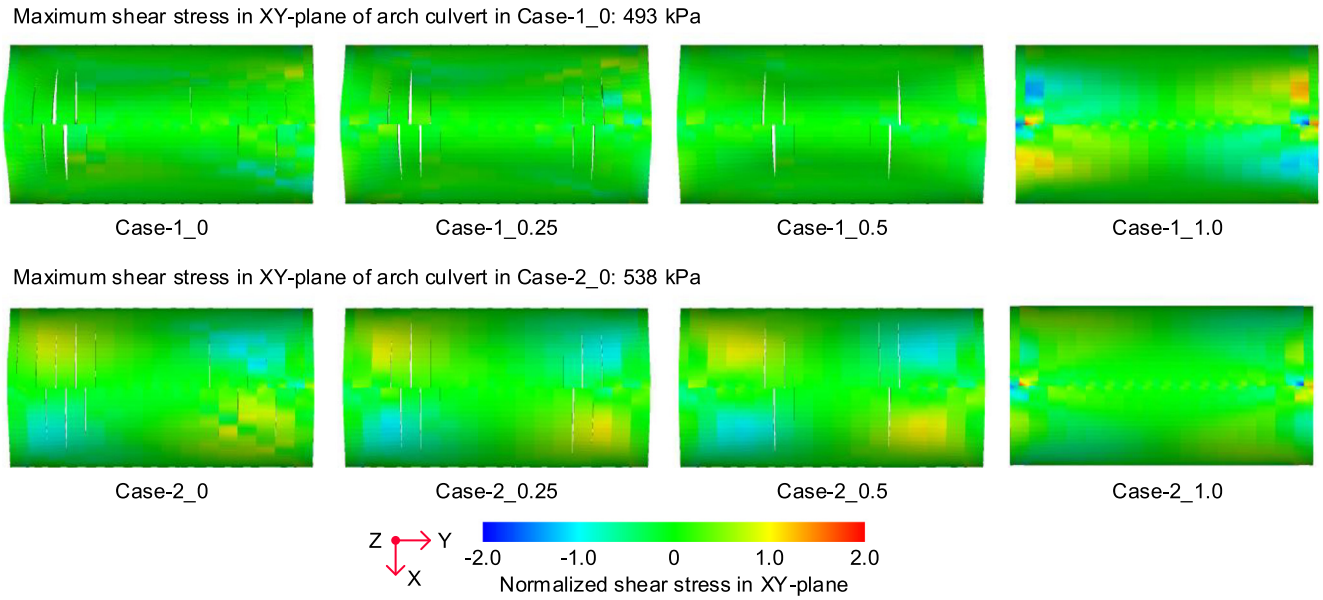


Fig. 19. Heatmaps of normalized $\tau_{xy}$ of arch members after excitation.

### 5.2. Discussion on assumed damage mechanism reported after the 2011 off the Pacific Coast of Tohoku Earthquake

Fig. 23 shows the stress states of the arches in Case-2_0 during excitation. According to the assumed damage mechanism in the 2011 off the Pacific Coast of Tohoku Earthquake (Fig. 5(b)), and focusing on the positional relation between the stress concentration on the arch crown and the arch foot, each zone of concentrated stress occurred on diagonal lines of the arch members, which proves the clear torsional deformation of the arch members. The analytical results in Case-2_0, which is the all longitudinally separated condition, exhibit similar stress related to the deformation state, as seen in Fig. 5.

The seismic wave, under which the culverts suffered damage, is likely to have a torsional vector considering the location of the culverts, as shown in Fig. 6, which is likely to amplify the torsional displacements of the arches. Moreover, little consideration was given to the seismic effect in the longitudinal structural connectivity of the damaged three-hinged culverts. The combination of this weaker structural connectivity and the torsional deformation of the arch members is likely to have induced the specific damage to the arch members, such as the edge defects in

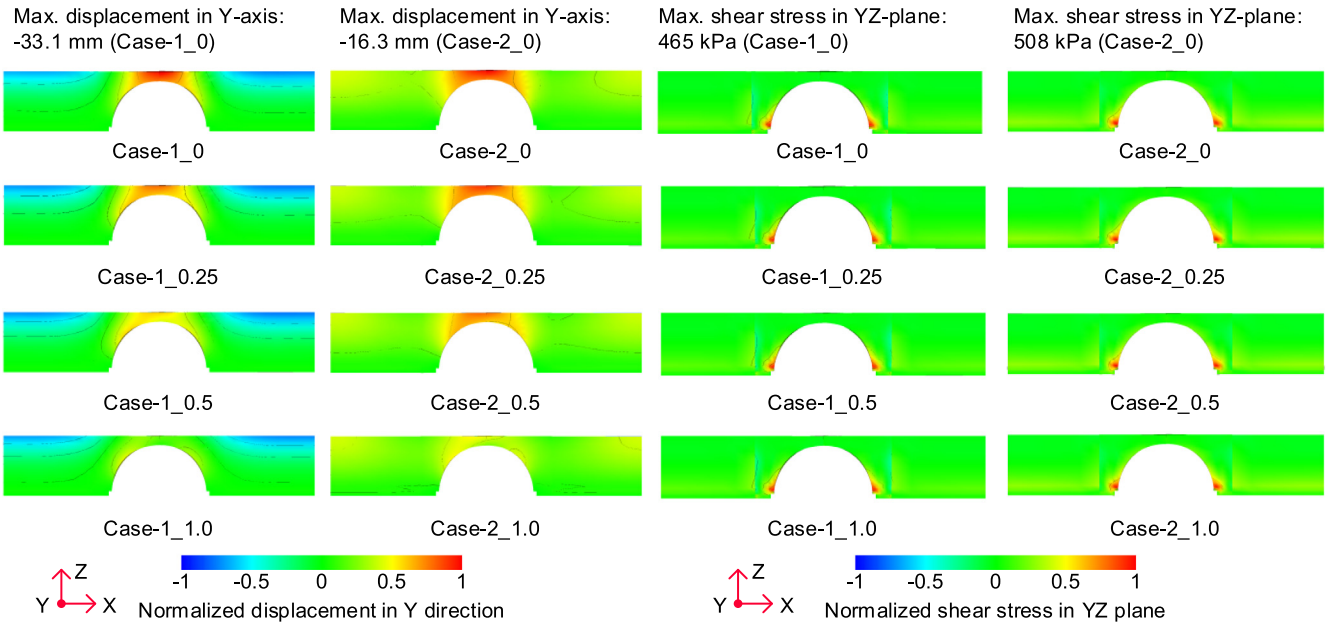


Fig. 20. Heatmaps of normalized displacements in Y-axis direction and $\tau_{yz}$ of mouth wall in Case-1 and Case-2.

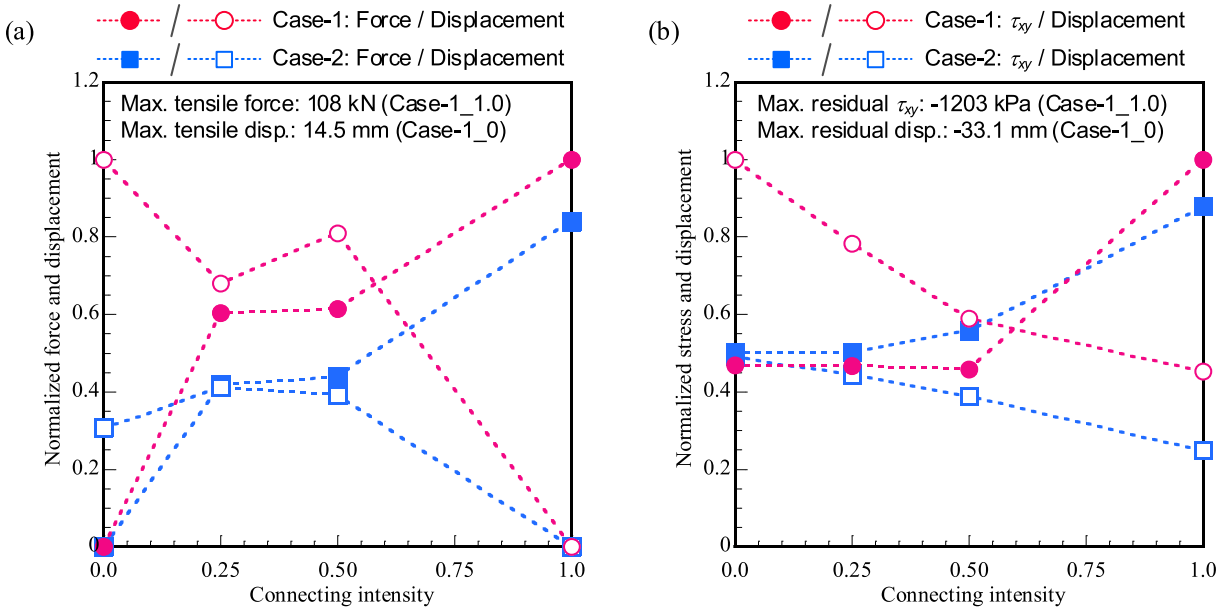


Fig. 21. Quantitative evaluation with connecting intensity for longitudinal seismic performance of three-hinged arch culverts: (a) Normalized maximum tensile displacements and forces on longitudinal connection and (b) Normalized maximum displacement in Y-axis direction of mouth wall and maximum $\tau_{xy}$ of arch members.

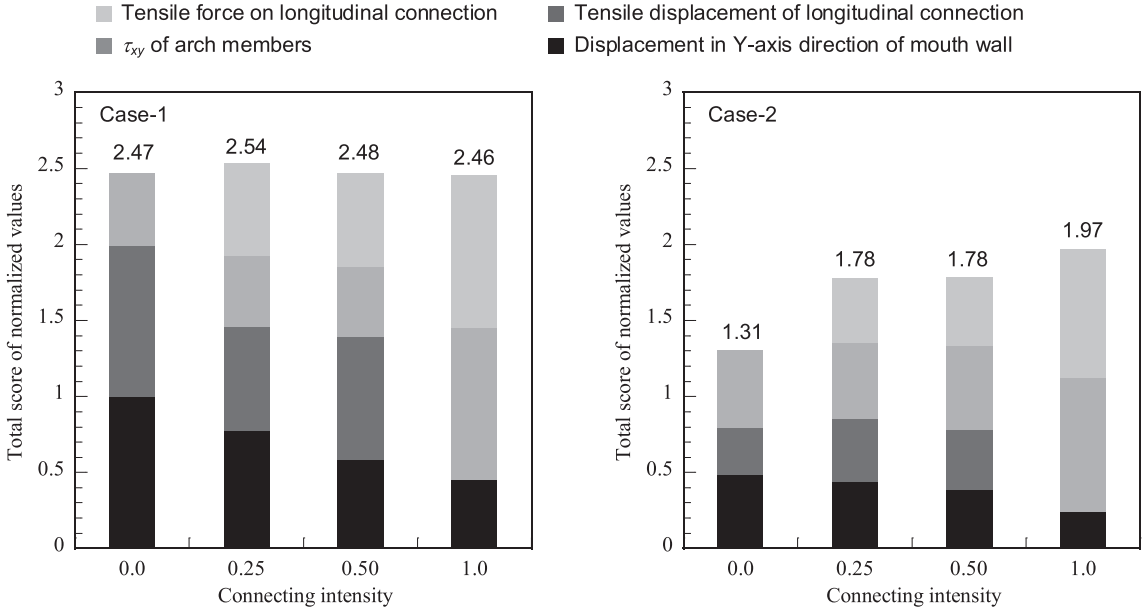


Fig. 22. Total scores of normalized values in accordance with different connecting intensities in Case-1 and Case-2. The total score of the normalized values is the sum of the normalized maximum tensile displacements of and the tensile forces on the longitudinal connection, normalized maximum $\tau_{xy}$ of the arch members, and the normalized maximum displacement in the Y-axis direction of the mouth wall. Each value given on the tops of the columns is the total score of the normalized values.

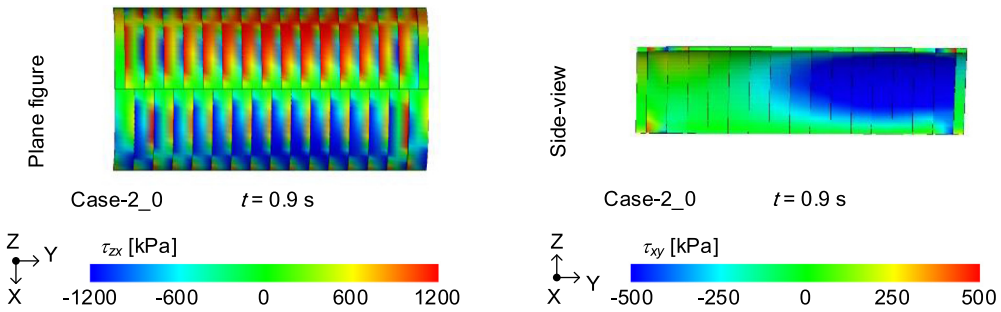


Fig. 23. Stress states of arches during excitation in Case-2_0.

the arch crown and the concrete foundation. These results clearly indicate the importance of the longitudinal structural connectivity in the seismic performance of three-hinged arch culverts.

## 6. Conclusions

The present study was implemented for the sake of clarifying how longitudinal structural connectivity contributes to the seismic behavior of three-hinged arch culverts. To achieve this objective, a simple elasto-plastic FEM analysis was conducted with a longitudinal earthquake. The longitudinal structural connectivity was expressed by the penalty method applied for the solutions of contact-impact problems between precast segmental arch members. The input wave was 1 Hz and 300 Gal, and there were three cycles of sinus waves. The obtained conclusions are as follows.

1. Under the input of a 1-Hz sinus wave, the deformation of the mouth wall was controlled by the displacements of the arch members, especially in the 1.0-m overburden condition, and the longitudinal structural connection was found to be important for decreasing the deformation of the mouth wall.
2. According to the overburden or the embankment shape condition, an appropriate longitudinal connected range was found to exist for decreasing the openings of the arches or the cross-sectional force on the arches. Therefore, considering what matters in the design phase, an appropriate longitudinal connected range should be selected. However, these appropriate conditions are likely to be dependent on the frequency and phase effect of the earthquake. Thus, the longitudinal dynamic behavior of various frequencies and phases should be considered in future studies.
3. It was confirmed that the damage mechanism suggested by Abe and Nakamura (2014) can be explained by a combination of the longitudinal seismic behavior of the three-hinged arch culverts and their weak longitudinal structural connection. In reality, the seismic wave which the damaged culverts experienced is likely to have a torsional vector considering the location of the culverts and based on the report by GSI (2011), which is likely to amplify the torsional displacements of the arches. Moreover, the damaged three-hinged arch culvert was an old type and did not have a concrete beam at the arch crown. The combination of this weaker structural connectivity and the torsional deformation of the arch members is likely to have induced the specific damage to the arch members, such as edge defects in the arch crown and the concrete foundation.

From these series of parametric studies on the longitudinal structural connectivity, as with tunnels, even the three-hinged arch culverts with shallow overburdens were seen to have a stronger correlation with the ground. Several studies remain to be discussed by sophisticatedly modeling the reinforced earth wall considering the reinforcements and verifying the correlation with the penalty method and mesh finesses under an actual recorded earthquake with complicated different frequencies. However, the full dynamic 3D analysis of the longitudinal seismic behavior in the present study has indicated the importance of the longitudinal structural connection in the seismic performance of three-hinged arch culverts.

## Acknowledgements

This work was supported by the RESEARCH FOUNDATION ON DISASTER PREVENTION OF EXPRESS HIGHWAY BY NEXCO-AFFILIATED COMPANIES.

## References

Abe, T., Nakamura, M., 2014. The use of and the caution in the application of the culvert constructed by large precast element in the expressway construction. Found. Eng. Equip. Month. 42 (4), 8–11 (in Japanese).

Asaoka, A., Noda, T., Yamada, E., Kaneda, K., Nakano, M., 2002. An elasto-plastic description of two distinct volume change mechanisms of soils. Soils Found. 42 (5), 47–57.

Association of Modularch Construction Method in Japan, 2017. Engineering Manual for Modularch, Geo-Research Institute (in Japanese).

Byrne, P.M., Anderson, D.L., Jitno, H., 1996. Seismic Analysis of Large Buried Culvert Structures. Transp. Res. Rec. 1541 (1), 133–139.

Cui, Y. Kishida, K. and Kimura, M., 2010. Analytical study on the control of ground subsidence arising from the phenomenon of accompanied settlement using footing reinforcement pile. Geotechnical Special Publication, Deep and Underground Excavation, ASCE, pp. 307–312. https://doi.org/10.1061/9780784411070.

Danno, K., Kimura, M., 2009. Evaluation of long-term displacements of pile foundation using coupled FEM and centrifuge model test. Soils Found. 49 (6), 941–958.

Geospatial Information Authority of Japan, 2011. Crustal Movements of Electronic Control Points Obtained from Continuous GPS Measurements, <http://www.gsi.go.jp/chibankansi/chikakukansi40005.html> (in Japanese).

Higo, Y., Lee, C.-W., Doi, T., Kinugawa, T., Kimura, M., Kimoto, S., Oka, F., 2015. Study of dynamic stability of unsaturated embankments with different water contents by centrifugal model tests. Soils Found. 55 (1), 112–126.

Hokyodo net service: Construction examples of Techspan construction method (access on 2014/10/10): <https://www.hokyodo.jp/2_pa/frame.html> (in Japanese).

Hutchinson, D., 2004. Application and design of segmental precast arches, Geotechnical Engineering for Transportation Projects, Geo-Trans 2004, ASCE Geotechnical Special Publication, pp. 452–459.

Hughes, T.J.R., Taylor, R.L., Sackman, J.L., Curnier, A., Kanoknukulchai, W., 1976. A finite element for a class of contact-impact problems. Comput. Methods Appl. Mech. Eng. 8, 249–276.

Japan Road Association, 2010. Road Earthwork Guidelines – Guidelines for Culvert Work (in Japanese).

Japan Road Association, 2012. Specifications for Highway Bridges Vol. V: Seismic Design.

Kazama, M., Noda, T., 2012. Damage statistics (Summary of the 2011 off the Pacific Coast of Tohoku Earthquake damage). Soil Found. 52 (5), 780–792. https://doi.org/10.1016/j.sandf.2012.11.003.

Kawashima, K., 2000. Seismic design of underground structures in soft ground – a review, In: Kusakabe, Fujita, Miyazaki (Eds.) Geotechnical

Aspects of Underground Construction in Soft Ground, Balkema, Rotterdam, ISBN 90-5809-1-066.

Kono, D., Inagaki, T., Matsubara, A., Yamaji, I., 2013. Stiffness model of machine tool supports using contact stiffness. Precis. Eng. 37 (3), 650–657. https://doi.org/10.1016/j.precisioneng.2013.01.010.

Kumada, T., Takahashi, Y., Kitabayashi, T., Hotta, M., Ohi, J., and Koizumi, A., 1995. Shaking table test on a tunnel of Tekspan construction method (No. 1); outline of Tekspan construction method and shaking table test, the Proceedings of the JSCE Annual Meeting, vol. 65, III-556, pp. 1112–1113 (in Japanese).

Montgomery, C.J., Morison,, R.M., Channen, J.R., Tutty, D.O., 1993. Design and construction of a buried precast prestressed concrete arch. PCI J. 38 (1), 40–57. https://doi.org/10.15554/pcij10.15554/pcij.0101199310.15554/pcij.01011993.40.57.

Miyazaki, Y., Sawamura, Y., Kishida, K., Kimura, M., 2017. Evaluation of dynamic behavior of embankment with precast arch culverts considering connecting condition of culverts in culvert longitudinal direction. Jpn. Geotech. Soc. Spec. Publ. 5 (2), 95–100.

Miyazaki, Y., Sawamura, Y., Kishida, K., Kimura, M., 2018. Dynamic behavior of three-hinge type precast arch culverts installed in embankment with various patterns of overburden in culvert longitudinal direction. In: Proc. of the 9th International Conference on Physical Modelling in Geotechnics, London, United Kingdom, pp. 915–920.

National Institute for Land and Infrastructure Management and Public Works Research Institute (NILIM and PWRI), 2006. Road facilities, Report on Damage to Infrastructures by the 2004 Mid Niigata Prefecture Earthquake, pp. 59–62 (in Japanese).

Ojima, H., Sato, M., 2011. Damage to precast arch culvert. In: Proceedings of The 29th Japan Road Conference, No. 4003 (in Japanese).

Owen, G.N., Scholl, R.E., 1981. Earthquake engineering of large underground structures, Report No. FHWA/RD-80/195, Federal Highway Administration and Natural Science Foundation.

Public Works Research Institute (PWRI), Nippon Expressway Research Institute Company Limited (NEXCORI) and Graduate School of Engineering, Kyoto University, 2020. Report on Evaluation of Seismic Performance and Anti-seismic Reinforcement of Constructed Culverts with Precast Concrete Members, No. 1 (in Japanese).

Sasaki, T., Sugita, H., Ohkawa, H., Mizuhashi, M., 2008. Ground investigation of the embankments damaged by the 2007 Noto Hanto Earthquake. In: The 63rd Annual Meeting of JSCE, Sendai, September10–20, CD-ROM, disc1, 3-034, pp. 67–68 (in Japanese).

Schofield, A.N., Wroth, C.P., 1968. Critical State Soil Mechanics. McGraw-Hill, London.

Sawamura, Y., Kishida, K., Kimura, M., 2015. Centrifuge model test and FEM analysis of dynamic interactive behavior between embankments and installed culverts in multiarch culvert embankments. Int. J. Geomech. ASCE 15 (3), 04014050. https://doi.org/10.1061/(ASCE)GM.1943-5622.0000361.

Sawamura, Y., Ishihara, H., Kishida, K., Kimura, M., 2016a. Experimental study on damage morphology and critical state of three-hinge precast arch culvert through shaking table tests. Proc. Eng. Adv. Transport. Geotech. III 143, 522–529.

Sawamura, Y., Ishihara, H., Kishida, K., Kimura, M., 2016b. Evaluation of damage morphology in three-hinge precast arch culvert based on shaking table tests and numerical analyses. In: Proc. of the 8th Young Geotechnical Engineering Conference, pp. 221–226, Astana, Kazakhstan.

Sawamura, Y., Matsushita, R., Kishida, K., Kimura, M., 2017. Evaluation of mechanical behavior of two-hinge precast arch culvert in construction process and its seismic damage morphology through strong earthquake response experiments. Jpn. Geotech. J. 15 (4), 385–396. https://doi.org/10.3208/jgs.12.385 (in Japanese).

Sawamura, Y., Ishihara, H., Otani, Y., Kishida, K., Kimura, M., 2019. Deformation behavior and acting earth pressure of three-hinge precast arch culvert in construction process, Underground Space, vol. 4(3), pp. 251–260. https://doi.org/10.1016/j.undsp.2018.09.005.

Segrestin, P., Brockbank, W.J., 1995. Precast arches as innovative alternate to short span bridges. Proc. Fourth Bridge Eng. Conf. 2, 219–226.

Seto, H., Ootani, Y., 2014. Outline of and construction example of Techspan construction method. In: The Foundation Engineering & Equipment, Monthly, vol. 42, no. 4, pp. 8–11(in Japanese).

Soba, T., Hootta, M., Ota, H., 1997. Measurement and construction of precast arch method (Techspan) (No. 1). In: Proceedings of The 22nd Japan Road Conference, pp. 58–59 (in Japanese).

Suzuki, N., Toi, Y., 1987. Finite element analysis of dynamic frictional contact problems by using the penalty function method -consideration on the penalty numbers and its application to the friction-excited vibration problem. J. Soc. Naval Arch. Jpn. 1987 (162), 364–373.

Tamura, C., Okamoto, S., Hamada, M., 1975. Dynamic behavior of a submerged tunnel during earthquakes. Institute of Industrial Science Report, vol. 24, no. 5, University of Tokyo, Tokyo.

Technical Committee of Manual for the Design and Construction of Tekspan Construction Method in Japan, 1998. Manual for the Design and Construction of Tekspan Construction Method (Draft), Advanced Construction Technology Center (in Japanese).

Toyota, H., Takagai, M., 1999. Dynamic behavior of 3-hinge arch in terre armee foundation, J. JSCE, No. 624/III-47, pp. 255–266. https://doi.org/10.2208/jscej.1999.624_255 (in Japanese).

Toyota, H., Ito, T., 2000. Effects of shaking conditions and material properties on dynamic behavior of terre armee foundation and 3-hinge arch, J. JSCE, No. 666/III-53, pp. 279–289. https://doi.org/10.2208/jscej.2000.666_279 (in Japanese).

Wang, J.N., 1993. Seismic Design of Tunnels – A Simple State of the art Design Approach. New York: Parsons Brinckerhoff Inc.

Wood, J.H., Jenkins, D.A., 2000. Seismic analysis of buried arch structures. In: Proc. of the 12th World Conference of Earthquake Engineering, No. 0768.

Ye, B., Ye, G., Zhang, F., Yashima, A., 2007. Experiment and numerical simulation of repeated liquefaction-consolidation of sand. Soils Found. 47 (3), 547–558.

Zhang, F., Ye, B., Noda, T., Nakano, M., Nakai, K., 2007. Explanation of cyclic mobility of soils, approach by stress-induced anisotropy. Soil Found. 47 (4), 635–648. https://doi.org/10.3208/sandf.47.635.